2018 International Conference on Indoor Positioning and Indoor Navigation (IPIN), 24-27 September 2018, Nantes, France

Indoor Positioning using OFDM-based Visible Light Communications Systems

Birendra Ghimire, Jochen Seitz, Christopher Mutschler
Fraunhofer Institute for Integrated Circuits IIS, Erlangen, Germany
Email: birendra.ghimire@iis.fraunhofer.de

***Abstract*—A novel indoor positioning approach using entities of the visible light communication system as anchor points and tags is presented. Time difference of arrival between anchor points and tags is estimated by means of positioning reference signals embedded into the orthogonal frequency division multiplexing (OFDM)-based visible light communication air interface, assuming a joint processing of signals transmitted by the anchor points. Simulation results show that positioning accuracy of 10 cm or higher is possible for over 95% of users given a sampling clock offset better that 10 ppm, clock jitter below 1 ps and a bit resolution of 16 bits.**

I. Introduction

Current advances in development in field of automation have placed greater demand on precision of the computation of the position of the object being tracked, both in indoor and outdoor scenarios. Global navigation satellite system (GNSS) is the most ubiquitous positioning system in outdoor scenario which is used for civilian and military uses alike. Of the most popular GNSS, global positioning system (GPS) achieves a measured mean accuracy of 5 m in horizontal plane using commercially available smartphones [1]. An accuracy of 5 m may be sufficient for the most ubiquitous use of navigating a person or a vehicular traffic from its source to destination. However, such accuracy is insufficient in the context of autonomous driving or autonomous drone navigation [2]. To improve accuracy, advanced receiver architectures that combine range measurements from GNSS satellites with measurements of motion and orientation with inertial sensor units are being developed.

Likewise, in an indoor scenario, the stringent demand on positioning is fuelled in part by the growth in Internet-of-Things (IoT)-applications [3]. Especially in the context of the fourth revolution in the industry, popularly termed Industry 4.0, it has become essential that the objects are able to ascertain either their absolute or their relative surroundings and form networks in order to interact with one another. One particular example could be tracking of location of tools and persons in a factory [4], so as to ensure certain quality control parameters of a process are fulfilled. Likewise, storing and retrieving goods in a warehouse, moving a mobility-impaired person from a room to another in hospitals, stations, airports could be other applications in an indoor environment that require precise determination of position and communication.

While indoor positioning is a topic of intensive research and development, there is no single standard or system for positioning in indoor scenario. Seamless coverage with GNSS is not feasible due to weak coverage of GNSS signal indoors. Hence, a wide variety of systems are developed ranging from wireless local area network (WLAN) fingerprinting [5–7], proximity detection using bluetooth beacons [8] and ultra wide band (UWB) positioning systems [9, 10]. One of the major problem surrounding the signals in the Gigahertz band is multipath propagation, which limits the precision.

Optical signals, by contrast, are much more immune to multipath since the strength of the diffused component is significantly weaker than the direct path. As a result, high precision system in indoor scenario typically employ signals on or near the visible spectrum of the electromagnetic spectrum. The recent development in visible light communication (VLC) technology, which is considered to be one of the key-technologies driving the fifth generation (5G) of mobile communications is a suitable technology to be exploited for positioning in indoor scenario [11]. Techniques such as fingerprinting of optical signals from various anchors [12, 13], trilateration based on received signal strength [14, 15] or triangulation using imaging receivers [16] have been investigated. Visible light positioning systems have also been deployed commercially [17] in recent years. In addition, there have been reference positioning system based on camera that provide accuracy in the millimeter to centimeter region [18–20]. Likewise, time difference of arrival (TDOA)-based methods for positioning in the visible light communications are also considered indoor positioning [21]. However, the proposed methods are either difficult to scale or do not integrate seamlessly with the modern VLC systems that allow for multi-user support.

To address the above shortcomings and to utilise the VLC system for both positioning and communications, a method for estimating phase based on pilot signals is investigated in this paper. The proposed method requires that the VLC-capable anchors emit synchronised OFDM signals, where the modulated symbols are identical on data subcarriers, but on the subcarriers bearing positioning reference signals, they are unique to each anchor points (APs). By estimating the relative phase, the TDOA between any two anchors is computed and the position is computed using well-known TDOA-based algorithm such as [22]. The result show that a position error of less than 10 cm is feasible for more than 95% of the cases even when taking imperfections in clock signals and limited

bit resolution into account.

The remainder of the paper is arranged as follows: Section II provides a brief overview of the TDOA algorithm and VLC technology. Section III describes the system considered. The methodology and simulation parameters for the investigation are provided in Section IV-A and the results are provided in Section IV. Finally the conclusions are drawn in Section V.

II. System Description

Positioning of tags in an area where a VLC system is deployed is the focus of this work. The downlink transmission in an OFDM-based VLC system is used for computing the position of a tag. The coverage area of a VLC communication system is an attocell. A VLC-capable tag connects to an attocell that provides the strongest reception. At the same time, it also receives signal from nearby attocells. Fig. 1 shows the arrangement of anchors in a deployment area. The tag then analyses the visible light signals and computes the time delay between itself and each of the anchor points. The coordinates of the anchors in a local coordinate frame are assumed to be known to the tag. This information can be provided by the VLC system itself using a system information broadcast (SIB), the tag can compute its position using the well-known TDOA algorithm.

A brief discussion of TDOA algorithm and the OFDM-based VLC is provided.

A. TDOA-based positioning

TDOA [22] is a multilateration-based positioning technique where the difference in time of arrival (ToA) of signal are used to solve the unknown $x-$, $y-$ and $z-$coordinates of the tag. Denoting the time of flight (ToF) between anchor a and the tag as τ_a, x_a, y_a, z_a as $x-$, $y-$ and $z-$coordinates of the anchor a, the unknown coordinates x, y and z of the tag can be computed by solving

$$A_a x + B_a x + C_a z + D_a = 0\,. \tag{1}$$

The coefficients in (1) are defined as follows

$$\begin{aligned} A_a &= \frac{2x_a}{c\tau_a} - \frac{2x_1}{c\tau_1} \\ B_a &= \frac{2y_a}{c\tau_a} - \frac{2y_1}{c\tau_1} \\ C_a &= \frac{2z_a}{c\tau_a} - \frac{2z_1}{c\tau_1} \\ D_a &= c\tau_a - c\tau_1 - \frac{x_a^2 + y_a^2 + z_a^2}{c\tau_a} + \frac{x_1^2 + y_1^2 + z_1^2}{c\tau_1}. \end{aligned}$$

where c is the speed of electromagnetic waves through the air and $2 \leq a \leq N_A$, where N_A is the number of anchors in the system. If the $\tau_a \in \{\tau_1 \cdots \tau_{N_A}\}$, where $N_A \geq 5$ can be estimated and if, then the minimum mean square error (MMSE) position solution can be computed. The focus of this work is to compute the delays using optical wireless communication system. To this effect, the relevant details of the VLC system is briefly described below.

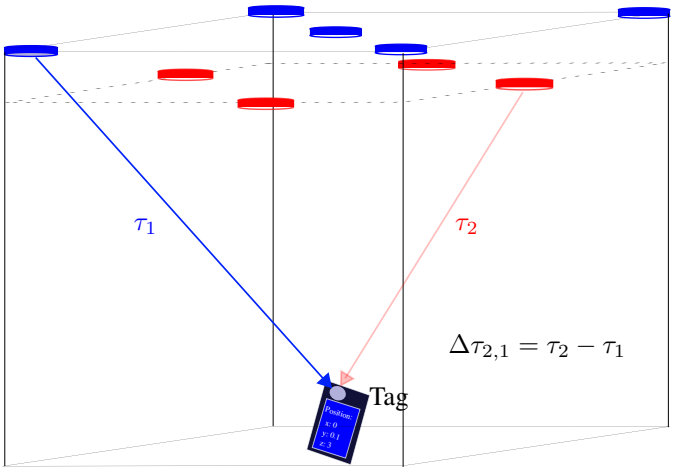

(a) Side view of the room

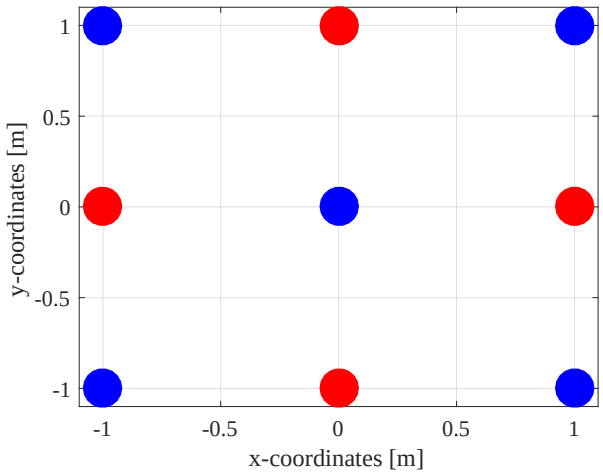

(b) Top view of the room

Fig. 1. Depiction of positioning with visible light communication network deployed in a room. (a) shows the side view and (b) shows the top-view. The APs are arranged in the ceiling in two groups with a height difference of δh. The arrangement of individual AP within a group is in a pre-defined pattern shown in (b).

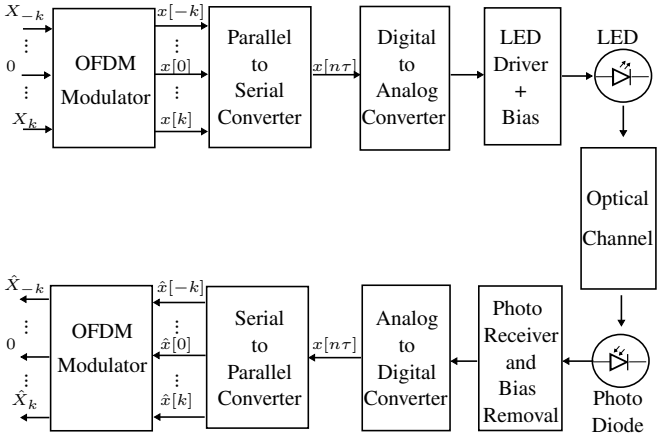

Fig. 2. Simplified depiction of OFDM-based VLC system.

B. OFDM-based VLC

Fig 2 [16, 23–25] depicts the essential components of a VLC system. The incoming bitstream is mapped into baseband symbols and each baseband symbol is modulated to a subcarrier. The available bandwidth B is divided into N subcarriers as shown in Fig.3. By taking N-point inverse discrete Fourier transform (IDFT) of the baseband symbols, the symbols are modulated onto the orthogonal subcarriers. In general, the input and output of discrete Fourier transform (DFT) operation are complex. However, as the light intensity emitted can only be real and positive, this requires special consideration in modulating the subcarriers. In particular, if the baseband symbol modulated onto the k^{th} subcarrier is denoted X_k, where $k \in \{-\frac{N}{2}, \ldots, \ldots, 0, \ldots, \frac{N}{2} - 1\}$, it is ensured that the output of an OFDM modulator is real if $X_k = X^*_{-k}$ holds [23]. The output of the OFDM modulator is digital to analog (D/A) converted and the requirement of positive optical intensity is ensured by adding a positive direct current (DC) offset to the OFDM symbol generated. The resultant signal is fed into an light emitting diode (LED) driver circuit, which converts the voltage fluctuations in the signal to fluctuations in the output intensity of light, a technique known as intensity modulation.

At the receiver side, the photodiode (PD) converts the light intensity into electrical signal. Since no heterodyne receivers are involved in conversion, the technique is known as direct detection. The current is amplified, sampled and analog to digital (A/D) converted. The baseband symbols are extracted by taking DFT of the samples and equalised with an expectation to recover the transmitted symbols.

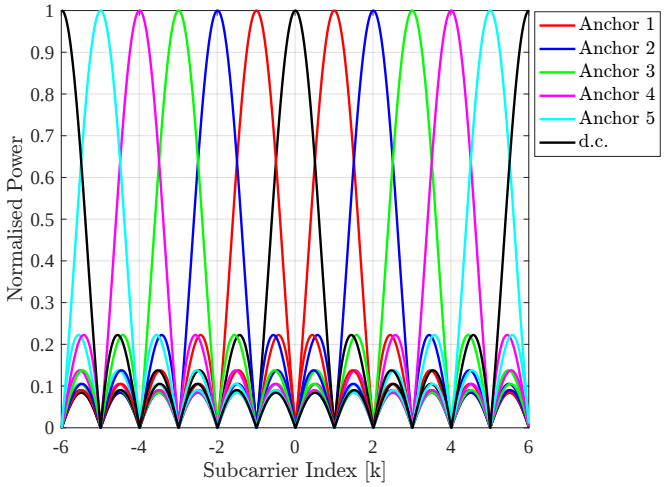

Fig. 3. Depiction of orthogonality of subcarriers in OFDM system. Only 16 subcarriers are depicted for clarity in visualisation. In OFDM-based VLC, the k^{th} and $-k^{\text{th}}$ subcarriers must be assigned to the same user to satisfy real-signal constraints.

III. System Design

The proposed system consists of APs controlled by a central controller, forming a cooperative multipoint (CoMP)

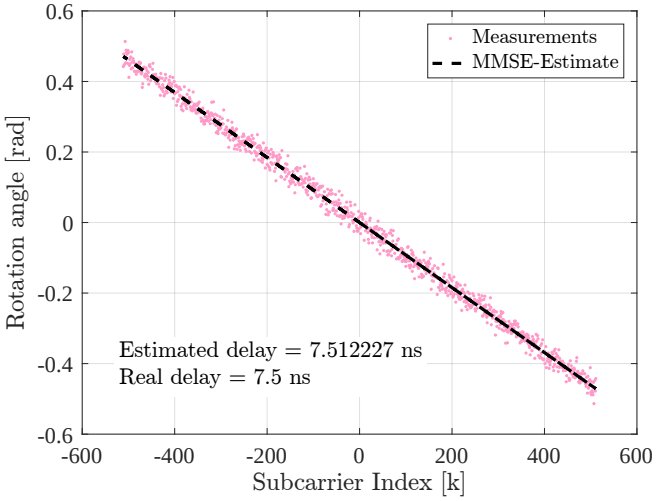

Fig. 4. Estimation of signal propagation delay from an APs to a tag.

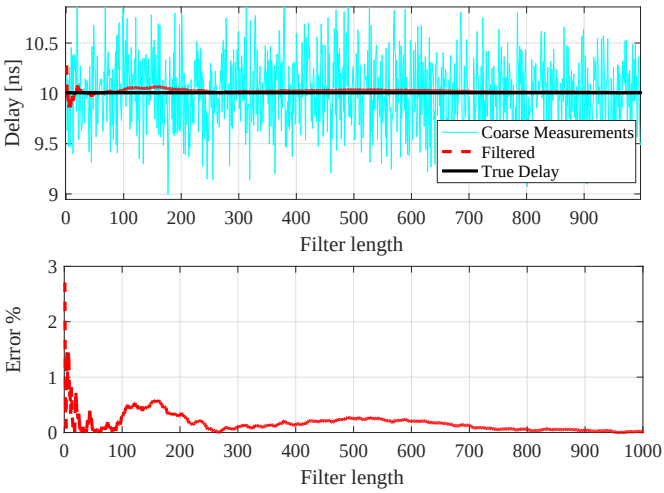

Fig. 5. Estimation of signal propagation delay from an APs to a tag.

system. The positioning reference signals are predetermined and allocated uniquely, at least locally, to each AP. The optical signals emitted from each of the APs travel through the optical channel and are received at the photo diode where they superimpose upon one another. The receiver is aware of the positioning reference signals allocated to each of the APs and extracts the signals and estimates the phases. Let the subcarrier $i \in \mathcal{P}_a$ be the set of subcarriers allocated to AP a for broadcasting the positioning reference signals and X_i be the positioning reference signal transmitted on the i^{th} subcarrier. The symbol transmitted by anchor a propagates through the optical channel and impinges upon the photodiode of tag b, where $H_i^{(a,b)}$ is the ideal channel response. The $\hat{X}_i^{(b)}$ is the received symbol at tag b on subcarrier i, the estimated channel response ($H_i^{(a,b)}$) is given by

$$\hat{H}_i^{(a,b)} = \frac{\hat{X}_i^{(b)}}{X_i^{(a)}}. \tag{2}$$

Noting that $\hat{X}_i^{(b)} = X_i^{(a)} H_i^{(a,b)} + \epsilon$, where ϵ is the error vector, (2) can be expressed as

$$\hat{H}_i^{(a,b)} = H_i^{(a,b)} + \epsilon H^{*(a,b)}_i. \tag{3}$$

The delay from AP a to tag b is denoted $\tau_{a,b}$, In the following, the subscript for tag b is dropped since there is no need to differentiate different tags within the scope of this paper. Hence τ_a represents the delay from AP a to tag b. The following relationship between τ and subcarrier index i holds:

$$\hat{H}_i^{(a)} = |H_i^{(a)}| e^{j\frac{2\pi}{\tau}\tau_a i} + \epsilon H_i^{*(a)} \tag{4}$$

In ideal sense, the phase of $H_i^{(a)}$ is linear with the subcarrier index i as depicted in Fig. 5. The gradient of the plot of subcarrier index i vs the phase of channel transfer function ($\angle H_i^{(a)}$) is

$$m = \frac{2\pi}{\tau}\tau_a. \tag{5}$$

Note that (5) is unique as long as $\tau_a < \tau$. However, provided the positioning reference signals are dense enough and uniformly positioned across the frequency domain, the phase jumps can be identified and the estimated phase can be linearly unwrapped. As a result, using (5) the value of τ_a can be estimated from $\hat{m}$, which is the noisy estimate of m using simple linear regression algorithm.

In order to investigate the impact of impairments, the source of estimation error on m are identified and investigated in this paper. In the following paragraphs, the prominent error sources are identified and discussed.

A. Quantisation noise

Quantisation noise in an ideal system where the signal uniformly spans entire A/D range is given by

$$\begin{aligned} \mathrm{SQNR} &= 10\log_{10}(2^Q) \\ &\approx 6.02 \cdot Q[\mathrm{dB}] \end{aligned} \tag{6}$$

where Q is the effective bit resolution of the A/D converter. In the proposed system, which employs joint processing at the anchors and constructive interference at the receiver, the strength of all signal components are not necessarily equal. The signal originating from the nearby AP suffers least quantisation noise and vice versa because the effective dynamic range of the A/D converter is determined by the strongest AP to avoid clipping of the signal.

B. Sampling clock offset and jitter

The received signal at the receiver in presence of mismatch between the transmitter and receiver clock frequency is modelled consistent with the author's earlier paper [24] as

$$\begin{aligned} \hat{X}_{i,l} &= X_{i,l} H_{i,l} \exp\left(\frac{j\pi(2i(lN_{\mathrm{os}} - N) + (i\Delta))}{N}\right) \cdot \\ &\quad \left(\frac{\sin(\pi(i\Delta))}{\sin(\frac{\pi}{N}(i\Delta))}\right) + \mathcal{N}_{\mathrm{CCI}} \end{aligned}$$

where $X_{i,l}$ and $Y_{i,l}$ are the transmitted and received baseband symbols on the i^{th} subcarrier during the l^{th} OFDM symbol. $H_{i,l}$ is the corresponding channel transfer function, N_{os} is the number of samples including the guard interval, N is the fast Fourier transform (FFT) window size and Δ is the mismatch between receiver and transmitter clocks. The term $\mathcal{N}_{\mathrm{CCI}}$ models the co-channel interference (CCI) noise [24], which is given by

$$\begin{aligned} \mathcal{N}_{\mathrm{CCI}} &= X_{i,l} H_{i,l} \cdot \\ &\quad \exp\left(\frac{j\pi(2k(lN_{\mathrm{os}} - N) + (k(\Delta+1) - i))}{N}\right) \cdot \\ &\quad \left(\frac{\sin(\pi(k\Delta + k - i))}{\sin(\frac{\pi}{N}(k\Delta + k - i))}\right) + \mathcal{N}_{\mathrm{jitter}}, \end{aligned}$$

where term N_{jitter} is noise caused due to clock jitter. The clock jitter is caused due to thermal noise at the sampling clock input of the A/D converter and is modelled as Gaussian noise. The clock jitter with stable clocks typically lies in the range of a few ps, which causes negligible errors in phase estimation in comparison to that caused by the sampling clock offset. The intersymbol intereference (ISI) is avoided by design in an OFDM system due to addition of guard interval and does not contribute to phase measurement errors.

C. Non-linear effects

Other non-linear effects including clipping and non-linear transmission characteristics of the LED are omitted for the scope of this publication. A comprehensive treatment of non-linear behaviour and their mitigation strategies can be found in [25]. Non-linear effects, other than the one specifically mentioned in this article are not modelled for the results presented in this simulations, and left as subject to further study.

D. Noise

VLC communication systems suffer from two categories of noise - first, the thermal noise and second the shot noise. The shot noise ($\mathcal{N}_{\mathrm{shot}}$), which originates in the photodiode is expressed as [16]

$$\mathcal{N}_{\mathrm{shot}} = 2qR_{\mathrm{p}}P_{\mathrm{opt}}B + 2qI_{\mathrm{bg}}I_2B, \tag{7}$$

where $q = 1.60217646 \times 10^{19}\,\mathrm{C}$ is electron charge, R_{p} is the responsivity of the photodiode, P_{opt} is the total optical power incident on the photodiode emitted by the anchors , B is the noise equivalent bandwidth, I_{bg} is the background current generated in the photodiode and I_2 is the noise bandwidth factor [16]. Likewise, the thermal noise which originates from the transimpedance amplifier, ($\mathcal{N}_{\mathrm{th}}$), is given by [16]

$$\mathcal{N}_{\mathrm{th}} = \frac{8\pi k_{\mathrm{B}} T}{G_{\mathrm{ol}}}\eta A_{\mathrm{pd}} I_2 B^2 + \frac{16\pi^2 k_{\mathrm{B}} T\Gamma}{g_{\mathrm{m}}}\eta^2 A_{\mathrm{pd}}^2 I_3 B^3, \tag{8}$$

where k_{B} is Boltzmann's constant, T is ambient temperature of the system, G_{ol} is the open loop voltage gain, η is the field capacitance per unit area, A_{pd} is the area of the photodiode, Γ is the channel noise factor of the field effect transistor (FET), g_{m} is the FET transconductance, and I_3 is the noise bandwidth factor.

The effect of noise on estimation of TDOA is considered, and the parameters used for generating the noise are provided in Table I.

E. Geometry of Anchor Location

The geometry of the anchor location influences the coefficients in (1). Consequently, for a given set of system imperfections, a certain geometrical setup of anchors provide may better positioning error than another setup. The setup in Fig 1 has been considered from the perspective of practicality of using the anchors as lighting devices, and no attempt has been made to enhance positioning accuracy due to anchor geometry.

IV. Results and Discussions

A. Simulation Setup

TABLE I
SIMULATION PARAMETERS

Parameter	Symbol	Value
LED transmit power	Var(X_k)	2.2 W
LED semi-angle	$\phi_{\frac{1}{2}}$	60°
FOV of the PD	ψ_c	90°
Surface area of the PD	A_{pd}	1cm^2
PD responsivity	R_p	0.5 A/W
Reflective index	n	1.5
Optical filter gain	T	1
Bandwidth	B	20 MHz
Background current	I_{BG}	5100 μA
Noise factor	I_2	0.562
Noise factor	I_3	0.0868
Circuit absolute temperature	T_K	295 K
Open-loop gain	G	10
FET Transconductance	g_m	30 mS
FET channel noise factor	Γ	1.5
Field capacitance per unit area	η	112pF/cm^2

The simulation parameters of the transmitter and receiver considered for the simulation are presented in Table I, consistent with [16]. The deployment scenario consists of a room where the AP emiting OFDM-modulated light signal are mounted towards the ceiling region in two horizontal planes, separated from each other by δh as depicted in Fig. 1(a). The two planes are depicted as a red grid and a blue grid in Fig. 1(b). The grid is formed by repeating a rhombus uniformly in the horizontal plane. The APs are placed at the vertices of the rhombus. The rhombus in the two planes are so arranged that the center of rhombus from one planar grid corresponds to the vertex of rhombus from another planar grid. This is done to ensure the deployment can be extended in a regular pattern.

The tags are distributed in a plane located at a height h from the lower plane containing the anchors. For the results presented herein, 200 tags are distributed randomly in the horizontal plane. The received signal is processed to measure the TDOA between the closest 6 APs and the position is computed using the TDOA localisation algorithm described in section III. The difference between the actual position and the computed position is collected for each of the tag and the statistics are presented in sectionIV.

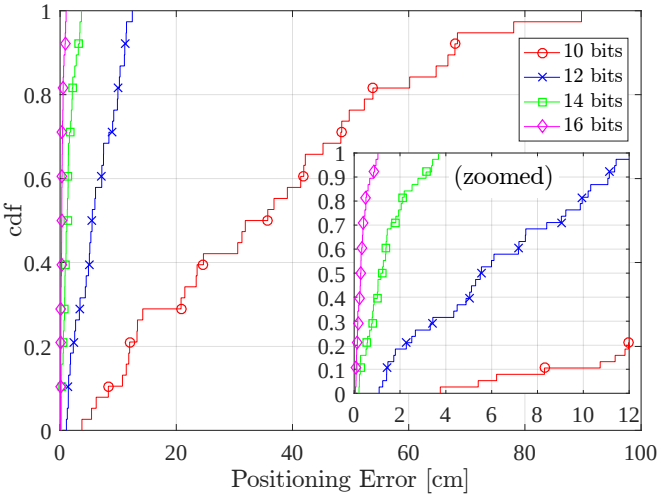

Fig. 6. Impact of quantisation on positioning error.

B. Impact of Quantisation Errors

The impact of quantisation on system performance is depicted in Fig. 6. For the results presented herein, other imperfections are ignored and only qunatisation error is considered. Four typical bit resolution of A/D converters are considered - 10 bits, 12 bits, 14 bits and 16 bits. The results show that the accuracy of the system degrades on reducing the bit resolution, as expected. In particular, it is observed that the accuracy at the 90^{th} percentile is 70 cm, in which case the benefits of TDOA system is lost and the performance is comparable to simply reading the cell ID broadcasted by the optical transmitter. The result show that bit resolution of 12 or higher is required to achieve sub-decimeter level accuracy envisaged for IoT applications. For the rest of the results in this paper, a bit resolution of 16 bits is assumed for two reasons - first, A/D converters of 16 bits resolutions and 20 MHz bandwidth are commercially available and second, for the algorithm using 16 bits resolution allows accuracy better than 1 cm in absence of clock imperfections.

C. Impact of Clock Imperfections

The impact of the clock impairment parameters, clock offset and jitter, as discussed in Section III-B on the accuracy of the system is presented in Fig. 7. For both systems, perfect synchronisation is assumed at the beginning and the synchronisation drifts as time passes by, and the receivers need to regularly synchronise with the transmitters. The result show that reducing the clock impairment factors increases the accuracy and vice versa. In addition, the result also show that for a given clock impairment parameter, the error rate is statistically lower when the APs share the same clock signal as opposed to when the AP generate their own clock signal. In particular, a sub-decimeter level accuracy is achieved with clock offset of 10 ppm and jitter with a standard deviation of 1 fs.

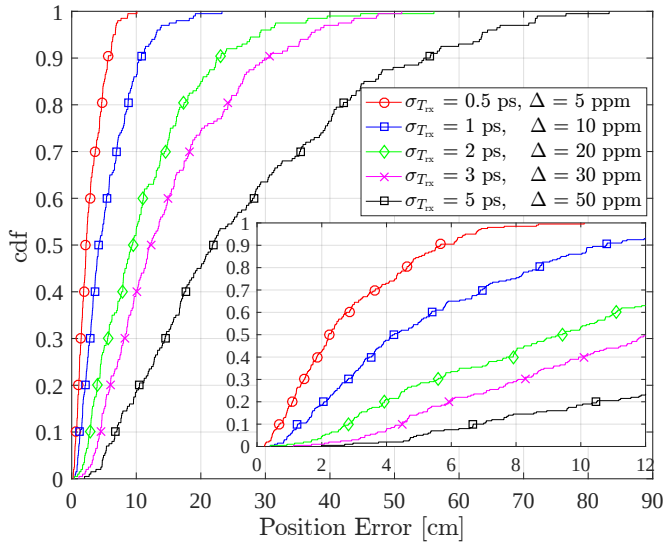

(a) Distributed clock generator

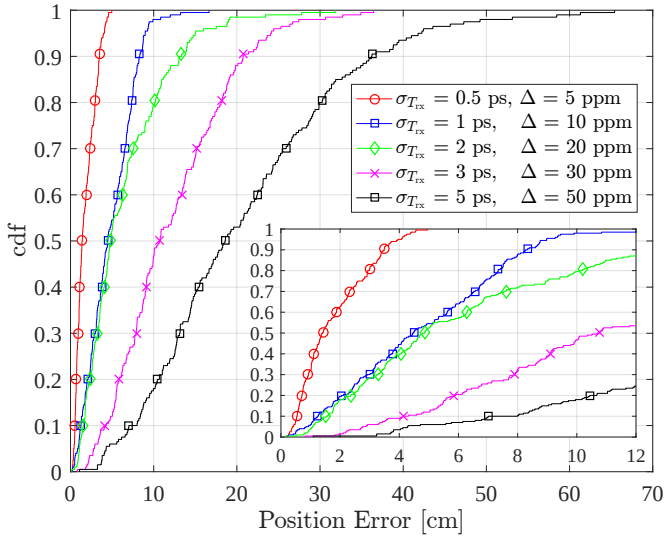

(b) Master clock

Fig. 7. Depiction of impact of different methods of clock signal generation at anchors on the system performance.

D. Spatial distribution of Errors

The spatial distribution of root mean square (rms) positioning error is plotted as a contour as a function of $x-$ and $y-$ coordinates. Tags are distributed at fixed location in a grid with a spacing of 10 cm and at each position the resultant error is computed. Four different systems parameters are considered - first, the performance of an ideal system is depicted in Fig 8(a), where only the thermal and shot noise are considered and the imperfections in system components are ignored, which shows that accuracy in milimeter region is possible with the proposed approach. The plots in Fig 8(b-d), show the system with resolution of 16 bits and a clock imperfection increasing from 1 ppm (b) to 5 ppm(d).

The horizontal and vertical components of the errors in position computation are plotted in Fig 9. The statistics are presented for the results presented in (d). The results show that the total error in position computation is dominated by the vertical component, which is expected because the maximum separation between two anchors is merely 10 cm in the vertical plane, as opposed to a minimum of 1 m in the horizontal plane. Nevertheless, a positioning error of less than 10 cm in horizontal domain can be obtained despite high clock impairment factors. Fusion of measurement from additional type of sensors, such as a high precision digital barometer [26, 27], could address the limitation arising due to insufficient vertical separation of anchors.

V. Conclusions

Indoor positioning using VLC has been investigated and shown that sub-decimeter level accuracy is possible. The impact of clock imperfections and quantisation on the accuracy of the positioning system is investigated. In particular, accuracy in 3D better than 10 cm is shown to be feasible if the sampling clock offset is kept below 10 ppm, clock jitter below 1 ps and bit resolution of 16 bits.

References

[1] F. van Diggelen and P. Enge, "The World's first GPS MOOC and Worldwide Laboratory using Smartphones," in *Proceedings of the 28th International Technical Meeting of The Satellite Division of the Institute of Navigation (ION GNSS+ 2015)*. Tampa, Florida, USA: ION, September 2015, pp. 361–369.

[2] M. Dorn, J. O. Filwarny, and M. Wieser, "Inertially-aided rtk based on tightly-coupled integration using low-cost gnss receivers," in *2017 European Navigation Conference (ENC)*, May 2017, pp. 186–197.

[3] D. Macagnano, G. Destino, and G. Abreu, "Indoor positioning: A key enabling technology for IoT applications," in *IEEE World Forum on Internet of Things (WF-IoT)*. Seoul: IEEE, 2014, pp. 117–118.

[4] "Intelligente werkzeuge in der montage." [Online]. Available: https://www.iis.fraunhofer.de/de/profil/jb/2017/iiot/werkzeugtracking.html

[5] S. Kram, C. Nickel, J. Seitz, L. Patino-Studencka, and J. Thielecke, "Spatial interpolation of wi-fi rss fingerprints using model-based universal kriging," in *2017 Sensor Data Fusion: Trends, Solutions, Applications (SDF)*, Oct 2017, pp. 1–6.

[6] R. Khullar and Z. Dong, "Indoor localization framework with wifi fingerprinting," in *2017 26th Wireless and Optical Communication Conference (WOCC)*, April 2017, pp. 1–6.

[7] C. BASRI and A. E. Khadimi, "Survey on indoor localization system and recent advances of wifi fingerprinting technique," in *International Conference on Multimedia Computing and Systems (ICMCS)*, Sept 2016, pp. 253–259.

[8] D. Namiot and M. Sneps-Sneppe, "On bluetooth proximity models," in *2016 Advances in Wireless and Optical Communications (RTUWO)*, Nov 2016, pp. 80–84.

[9] M. M. Pietrzyk and T. von der Grün, "Experimental validation of a toa uwb ranging platform with the energy detection receiver," in *2010 International Conference on Indoor Positioning and Indoor Navigation*, Sept 2010, pp. 1–8.

[10] S. N. A. Ahmed and Y. Zeng, "Uwb positioning accuracy and enhancements," in *TENCON IEEE Region 10 Conference*, Nov 2017, pp. 634–638.

[11] Y. Zhuang, L. Hua, L. Qi, J. Yang, P. Cao, Y. Cao, Y. Wu, J. Thompson, and H. Haas, "A Survey of Positioning Systems Using Visible LED Lights," *IEEE Communications Surveys Tutorials*, pp. 1–1, 2018.

[12] J. Vongkulbhisal, B. Chantaramolee, Y. Zhao, and W. S. Mohammed, "A fingerprinting-based Indoor Localization System using Intensity Modulation of Light Emitting Diodes," *Microwave and Optical Technology Letters*, vol. 54, no. 5, pp. 1218–1227, 2012. [Online]. Available: https://onlinelibrary.wiley.com/doi/abs/10.1002/mop.26763

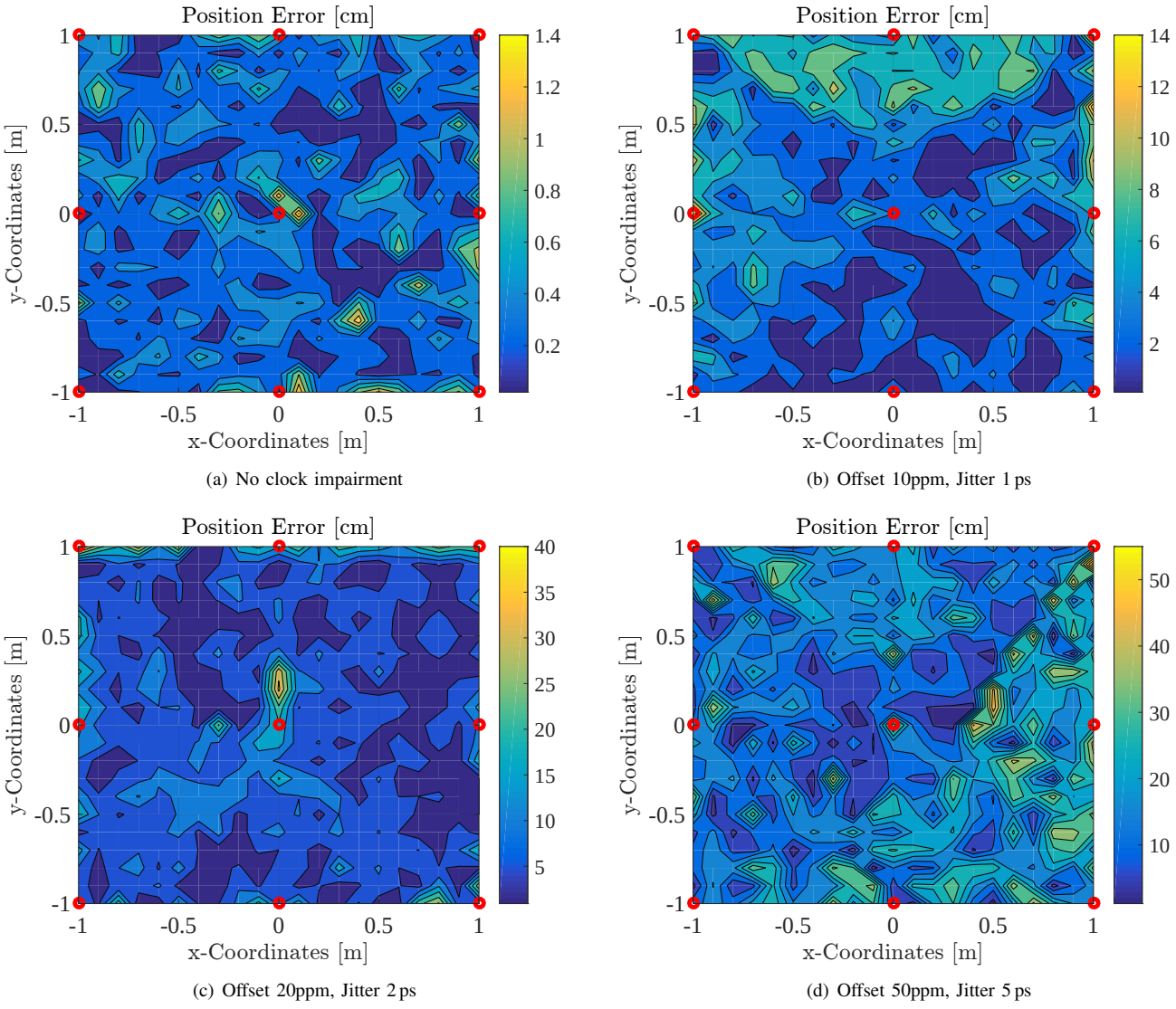

(a) No clock impairment

(b) Offset 10ppm, Jitter 1 ps

(c) Offset 20ppm, Jitter 2 ps

(d) Offset 50ppm, Jitter 5 ps

Fig. 8. Spatial distribution of rms error in position computation.

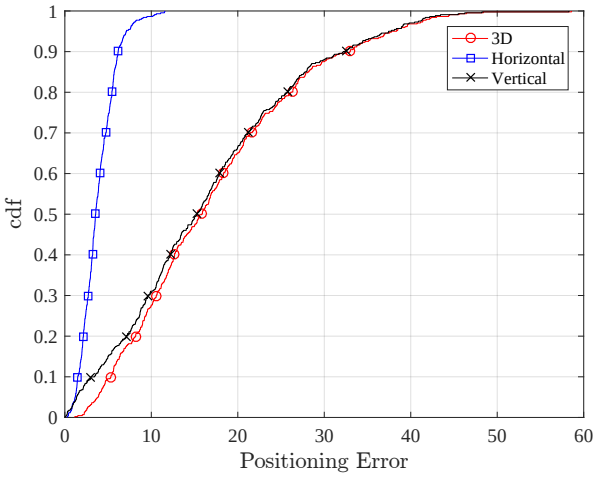

Fig. 9. Distribution of position error in horizontal and vertical plane.

[13] H. Wei and H. Yao, "Indoor visible light location algorithm based on virtual fingerprint database," in *Advanced Information Technology, Electronic and Automation Control Conference (IAEAC)*, March 2017, pp. 2412–2415.

[14] K. Moriya, M. Fujimoto, Y. Arakawa, and K. Yasumoto, "Indoor localization based on distance-illuminance model and active control of lighting devices," in *International Conference on Indoor Positioning and Indoor Navigation (IPIN)*, Alcala de Henares, Spain, Oct 2016, pp. 1–6.

[15] H. S. Kim, D. R. Kim, S. H. Yang, Y. H. Son, and S. K. Han, "An indoor visible light communication positioning system using a rf carrier allocation technique," *Journal of Lightwave Technology*, vol. 31, no. 1, pp. 134–144, Jan 2013.

[16] L. Yin, X. Wu, and H. Haas, "Indoor Visible Light Positioning with Angle Diversity Transmitter," in *Proc. of the Vehicular Technology Conference (VTC2015-Fall)*, Sept 2015, pp. 1–5.

[17] A. Jovicic, "Qualcomm Lumicast: A high accuracy indoor positioning system based on visible light communication," Qualcomm, White Paper, Apr 2016.

[18] "Nexonar Broschure - Products and Applications," http://www.nexonar.com/files/nex_broschuereanwendprod-2017-web.pdf retrieved 11.04.2018, Oct 2017.

[19] [Online]. Available: http://www.qualisys.com/applications/engineering/oem/, retrieved 11.04.2018

[20] [Online]. Available: https://ar-tracking.com/technology/technical-details/, retrieved 11.04.2018
[21] S. Y. Jung, S. Hann, and C. S. Park, "TDOA-based Optical Wireless Indoor Localization using LED Ceiling Lamps," *IEEE Transactions on Consumer Electronics*, vol. 57, no. 4, pp. 1592–1597, November 2011.
[22] Y. T. Chan and K. C. Ho, "A simple and efficient estimator for hyperbolic location," *IEEE Transactions on Signal Processing*, vol. 42, pp. 1905–1915, Aug 1994.
[23] M. S. Islim and H. Haas, "Modulation techniques for li-fi," *ZTE Communications*, vol. 14(2), pp. 29–40, April 2016.
[24] B. Ghimire, I. Stefen, H. Elgala, and H. Haas, "Time and Frequency Synchronisation in Optical Wireless OFDM Networks," in *Proc. of the IEEE 22nd International Symposium on Personal, Indoor and Mobile Radio Communications*. Toronto, ON: IEEE, Sept, 2011, pp. 819–823.
[25] R. Mesleh, H. Elgala, and H. Haas, "Led nonlinearity mitigation techniques in optical wireless ofdm communication systems," *Journal of Optical Communication Networking*, vol. 4, no. 11, pp. 865–875, Nov 2012. [Online]. Available: http://jocn.osa.org/abstract.cfm?URI=jocn-4-11-865
[26] *DPS310 Digital Barometric Pressure Sensor for Mobile and Wearable Devices*, Infineon Technologies AG, Munich, 2015.
[27] B. Ghimire, C. Nickel, and J. Seitz, "Pedestrian motion state classification using pressure sensors," in *2016 International Conference on Indoor Positioning and Indoor Navigation (IPIN)*, Oct 2016, pp. 1–6.